THE JOURNAL OF PHYSICAL CHEMISTRY B

Article

pubs.acs.org/JPCB

Computational Two-Dimensional Infrared Spectroscopy without Maps: *N*-Methylacetamide in Water

Pierre-André Cazade,[†] Tristan Bereau,[†,§] and Markus Meuwly*[,†,‡]

[†]Department of Chemistry, University of Basel, Klingelbergstrasse 80, 4056 Basel, Switzerland

[‡]Department of Chemistry, Brown University, Providence, Rhode Island 02912, United States

Supporting Information

ABSTRACT: The two-dimensional infrared spectrum of NMAH and NMAD in H_2O and D_2O is computed on the basis of force field parametrizations ranging from standard point charge (PC) to more elaborate multipolar (MTP) representations of the electrostatics. For the latter, the nonbonded parameters (MTP and van der Waals) were optimized to reproduce thermodynamic data. The frequency trajectory and frequency−frequency correlation function (FFCF) are determined from explicit frequency calculations on $\sim 10^6$ snapshots without using a more traditional "mapping" approach. This allows us to both sample configurations and compute observables in a consistent fashion. In agreement with experiment, the FFCF shows one very rapid time scale (in the 50 fs range) followed by one or two longer time scales. In the case of three time scales, the intermediate one is ≈0.5 ps or shorter, whereas the longest time scale can extend up to 2 or 3 ps. All interaction models lead to three time scales in the FFCF when fitted to an empirical parametrized form. When two time scales are assumed—as is usually done in the analysis of experimental data—and the short time scale is fixed to the τ_1 = 50−100 fs range, the correlation time τ_c from the simulations ranges from 0.7 to 1 ps, which agrees quite well with experimentally determined values. The major difference between MTP and PC models is the observation that the later decay times in the FFCF are longer for simulations with MTPs. Also, the amplitude of the FFCF is reduced when simulations are carried out with MTPs. Overall, however, PC-based models perform well compared to those based on MTPs for NMAD in D_2O and can be recommended for such investigations in the context of peptide and protein simulations.

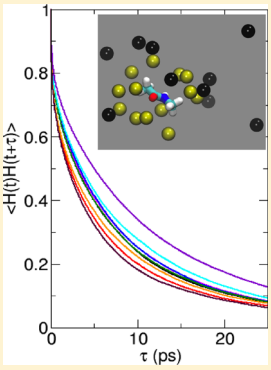

INTRODUCTION

Two-dimensional infrared (2D IR) spectroscopy is a powerful experimental technique providing detailed information on the structure and dynamics of condensed-phase systems.[1] Typically, one relies on a —CO or —CN chromophore, which is spectrally isolated from the other vibrational modes in the system of interest. A particular challenge in 2D IR experiments is the interpretation of the signal. To this end, detailed atomistic simulations can link experimentally observed dynamics to an underlying structural interpretation.

The utility of atomistic simulations depends on a number of essential prerequisites. The quality of the underlying computational model needs to be sufficiently accurate to provide a realistic description of the system's energetics—a challenging task, especially for solution-phase simulations. A quantum-mechanical description would provide the most rigorous representation. Unfortunately, computational limitations restrict the amount of sampling one can carry out. Typically, for isolated chromophores in solution, at least several nanoseconds of MD simulations are required which corresponds to 10^6 energy evaluations to be carried out. Therefore, one often resorts to more approximate force-field simulations, which allow for better sampling of configurational space. From the trajectory, one can then extract the frequency trajectory $\omega(t)$ of the oscillator of interest.

All the components of the third-order response from which the spectroscopic signal is determined[1] require the vibrational frequency $\omega(t)$ of the local oscillator. From a computational point of view, different approaches have been considered to determine $\omega(t)$ from MD simulations. Among them, electrostatic electronic structure (EES) considers electrostatic perturbations from the solvent to the electronic structure of the solute, whereas in optimized QM/MM (OQM/MM) the electrostatic parameters of a quantum method (such as PM3) are optimized to give agreement with the benchmark frequencies.[2] Alternatively, perturbation theory can be used to account for the vdW interactions while using ab initio calculations in the presence of an external electric field.[3,4] Despite excellent agreement with experiments for both the vibrational line shift and width for small systems (e.g., carbonyl stretch of acetone in acetonitrile), the computational cost limits the applicability to larger systems, such as peptides. Similarly, Mukamel and co-workers[5−7] developed an empirical ab initio map approach where the vibrational potential of the solute is expanded in normal-mode coordinates to a high order. The

Special Issue: James L. Skinner Festschrift

Received: February 2, 2014
Revised: March 13, 2014
Published: March 31, 2014

expansion coefficients are a function of the electrostatic potential generated by the solvent molecules, as well as its derivatives. In most cases, the agreement with experiments is very good. Since the frequencies depend on the solvent only via the inhomogeneous electrostatic potential and not its chemical identity, the approach is transferable.[8] However, the parametrization and validation of the maps requires significant effort, making it difficult to compute maps for larger systems. Another substitute to a fully ab initio treatment is the quantum mechanics/molecular mechanics QM/MM approach,[9−12] although applications to large systems remain difficult. Alternatively, one can estimate the frequency of vibration of the solute by solving the 1D Schrödinger equation.[13,14] This method requires an accurate potential energy surface or, similarly, a normal-mode analysis of the solute. Both methods are formally rigorous and rely on the MM potential used in the MD simulation. In addition to a consistent treatment between simulation and analysis, the computational cost remains reasonable, making the method applicable to large systems, e.g., peptides and proteins.

In the present work, a combination of sophisticated force field techniques, based on point charge and multipolar models, together with rigorous sampling of the conformational space to investigate the 2D IR spectroscopy of *N*-methylacetamide (NMA) is used. The C═O stretching vibration is the chromophore of choice for the IR probe of this system. NMA has been used repeatedly in experimental and computational studies and has become a standard to evaluate new IR technologies.[1,15−21] Previous computational work on NMA includes standard MD simulations with the AMBER force field with static charges and harmonic bonds and a QM/MM approach using the semiempirical PM3 method for the solute.[22] This work focused on spectroscopic signatures, though no detailed analysis of the frequency−frequency correlation function (FFCF) was provided. For the QM/MM simulations, quite good agreement with experiment was found, whereas purely classical simulations provide less satisfactory results. Alternatively, if the force field used for the simulations is sufficiently detailed, such a computational model can also be used to determine $\omega(t)$. In the present work, the second possibility is pursued.

This work is structured as follows: First, the computational methods, including the fitting and validation of the force fields employed, is described. Next, the 2D IR spectroscopy obtained from force fields of different origins and quality is compared by considering the frequency−frequency correlation function. For this, the frequency trajectory $\omega(t)$ of the C═O oscillator normal mode is determined by explicitly solving the 1D Schrödinger equation. Finally, the results are discussed in the light of previous simulations and experiments and atomistic aspects of the solvent dynamics are analyzed.

COMPUTATIONAL METHODS

The following summarizes the simulation methods together with the different parametrizations of the NMA chromophore, including a fluctuating-point-charge model (FPC) and several static atomic multipole (MTP) parametrizations, and finally several analysis tools.

Molecular Dynamics Simulations. All MD simulations were performed with CHARMM.[23] Parameters for NMA are based on CGenFF[24] and described in more detail below. For water, the TIP3P model was used.[25] Electrostatic interactions were computed using the particle-mesh Ewald (PME) method with a grid-size spacing of 1 Å, characteristic reciprocal length κ = 0.43 Å^{-1}, and interpolation order 4 for long-range electrostatics. A 12 Å cutoff was used for LJ and MTP interactions and simulations with the fluctuating point-charge model. The LJ and MTP interactions are switched at 10 Å whereas for the fluctuating point-charge model a shifting procedure was applied. The simulations were performed at T = 300 K and all bonds involving hydrogen atoms are constrained via the SHAKE algorithm.[26] Condensed-phase simulations—either NMA solvated in water or pure-liquid NMA—were carried out in cubic boxes of roughly 30 Å^3 with a density corresponding to that at ambient temperature and pressure. Standard minimization, heating, and equilibration procedures for ∼100 ps were employed to prepare the systems. Production simulations were run in the *NVT* ensemble, using the velocity-Verlet integration scheme and a Nosé−Hoover thermostat. The time step was Δt = 0.5 fs, and snapshots were recorded every 10 steps. In the simulations using MTPs, a Leapfrog integrator and constant temperature within the weak-coupling frame (coupling frequency 1 ps^{-1}) were employed.

MD simulations with multipolar interactions used the recently developed MTPL module[27] to compute MTP interactions in the atom's local frame.[28] The Hoover heat-bath method with pressure coupling was used for *NPT* simulations,[29] run at T = 373 K, P = 1 atm, and the masses of the temperature and pressure piston to 20 and 2% of the system's mass, respectively. A Langevin damping coefficient γ_p = 20 ps^{-1} was applied on the piston to equilibrate the box size. LJ long-range corrections were applied.[30] Density, heat of vaporization, and hydration free-energy (from thermodynamic integration) calculations were performed as described previously.[27]

Fluctuating Point Charge Force Field for NMAH. All quantum chemical calculations in the present work were carried out with the Gaussian software.[31] For the fluctuating point charge model, the structure of NMA was first optimized at the B3LYP/aug-cc-pVQZ level of theory. Subsequently, the structure of NMA was distorted along the C═O bond length r and the partial atomic charges were determined by means of fitting to the electrostatic potential (ESP).[32,33] The r-grid included 21 distances between r = 1.1 Å and r = 1.35 Å. This choice was motivated by the amount of fluctuations of this coordinate in the MD simulations (∼10%). All bonded interaction terms are those of the CHARMM22 force field,[34] except for the C═O stretching potential, which was optimized in two steps. First, the parameters of the Morse potential $V(r) = D_e(1 - \exp(-\beta(r - r_e)))^2$ are fitted to electronic structure data (B3LYP/aug-cc-pVTZ). The parameters are then refined by reproducing the experimental gas phase C═O stretch frequency of 1731 cm^{-1} by adjusting D_e.[35] The final parameters are then D_e = 120.47 kcal/mol, β = 2.174 Å^{-1}, and r_0 = 1.294 Å.

For each conformation, the charges obtained from the ESP-based fit are Taylor-expanded with respect to the equilibrium distance of C═O. Figure 1 shows the ESP-fit charges as a function of r for all heavy atoms. The dependence of each charge q_i on r is described by a linear expansion

$$q_X(r_{C=O}) = a_{X,0} + a_{X,1} r_{C=O} \quad (1)$$

where X stands for any atom of NMA (Table 1). Using the B3LYP/aug-cc-pVQZ level of theory to determine the necessary electrostatic parameters was found to be reliable in previous work for NO, CN$^-$, O_2, or CO_2.[36−40]

dx.doi.org/10.1021/jp5011692 | J. Phys. Chem. B 2014, 118, 8135−8147

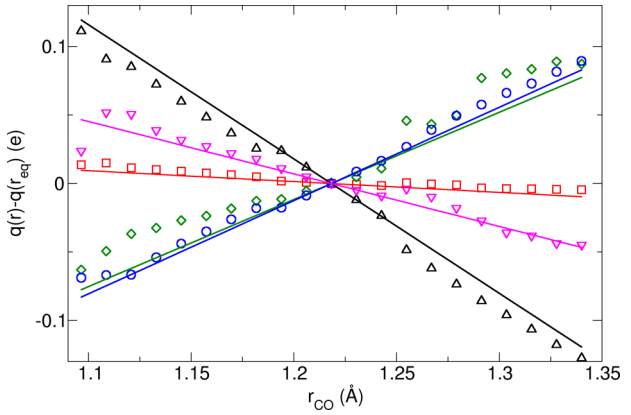

Figure 1. ESP charge variations of the atoms with respect to the C═O bond length for the heavy atoms: C (black △), O (red □), C(C═O) (green ◇), N (blue ○), C(N) (magenta ▽). The charges of each atom at $r^{eq}_{C=O}$ are used as reference values. Symbols are the data and solid lines the first-order fit.

Figure 2 shows the *ab initio* electrostatic field around NMA at the MP2 level. Two regions can be distinguished: a positive

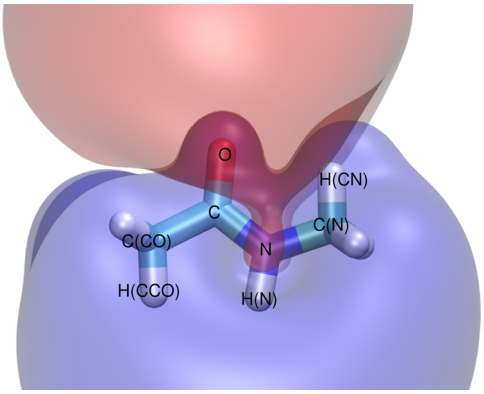

Figure 2. Isosurfaces of the *ab initio* electrostatic potential of NMA. Blue and red regions represent the interaction energy between a probe charge of +1*e* with the molecular field of +5 and −5 kcal/mol, respectively. Also, the atom types are indicated for further reference.

density (blue) which includes the hydrogenated parts of the molecule and a negative one (red) which mainly develops around the O atom with a small contribution on the N atom. These features need to be captured by a realistic model for the electrostatics, based either on point charge or multipolar representations.

Figure 3 compares the ESP generated by the *ab initio* electron density and the static (CGenFF) or fluctuating point charge models for varying C═O bond distances. It is found that both point charge models perform about equally well considering the extent and size of the difference maps. For the

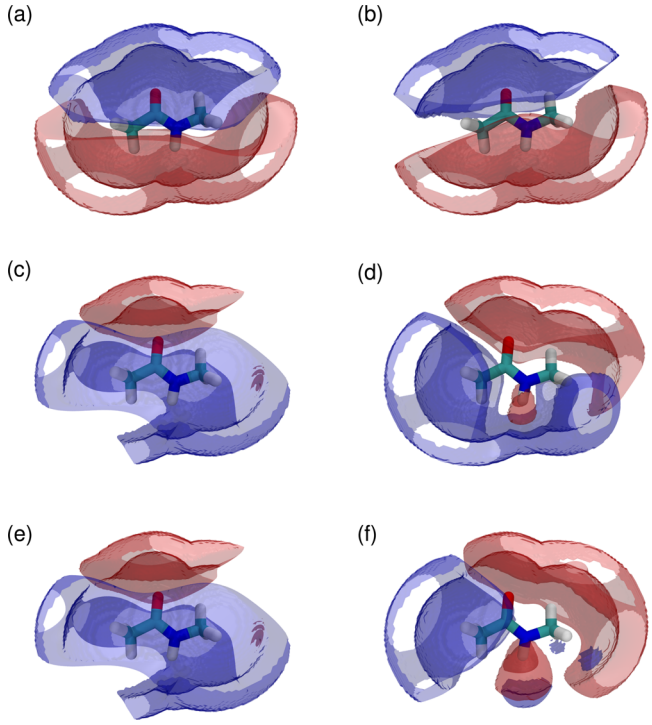

Figure 3. Difference between the ESP generated by the *ab initio* electron density and a set of point charges for varying C═O bond distances. *r*: low distance r_{min} = 1.17 Å, equilibrium distance r_{eq} = 1.23 Å, and large distance r_{max} = 1.32 Å. The point charges used are either from CGenFF or the fluctuating model. (a) CGenFF at r_{min}, (b) fluctuating charges at r_{min}, (c) CGenFF at r_{eq}, (d) fluctuating charges at r_{eq}, (e) CGenFF at r_{max}, and (f) fluctuating charges at r_{max}. The color coding represents isosurface errors of +0.5 and −0.5 kcal/mol in blue and red, respectively.

shortest distances, FPC is probably somewhat closer to the reference *ab initio* electron density. Another difference between the two parametrizations concerns the region around the N—H bond for the most elongated structure.

Multipolar Force Field for NMAH. The MTP parametrization of NMAH/NMAD was based on the CGenFF force field:[24] (i) all bonded interactions were kept identical, (ii) the MTP parameters were constrained to mimic the CGenFF point charges (PCs), and (iii) the Lennard-Jones (LJ) coefficients were fine-tuned to keep a number of thermodynamic properties intact. In the following, it is described how and to what extent both the electrostatics and the LJ interactions are varied, followed by a set of validating calculations.

MTP coefficients were fitted to the *ab initio* ESP using second-order Møller−Plesset theory and an aug-cc-PVDZ basis set. This level of theory has been used in recent work following the same parametrization protocol as that employed in the present work and differs from that for the FPC model above.[27]

Table 1. Electrostatic Parameters for the Point Charge Models of NMA[a]

model		C	O	C(C═O)	N	C(N)	H(CC═O)	H(N)	H(CN)
FPC	q_i	0.71	−0.57	−0.71	−0.43	−0.03	0.19	0.28	0.06
	$a_{i,0}$	1.90	−0.47	−1.47	−1.26	0.44	0.27	0.30	−0.08
	$a_{i,1}$	−0.98	−0.08	0.64	0.68	−0.38	−0.07	−0.02	0.12
CGenFF	q_i	0.51	−0.51	−0.27	−0.47	−0.11	0.09	0.31	0.09

[a]Units are *e* for charges q_i, *e* for coefficients $a_{i,0}$, and *e*/Å for $a_{i,1}$.

dx.doi.org/10.1021/jp5011692 | J. Phys. Chem. B 2014, 118, 8135−8147

Table 2. MTP Calculations of Pure-Liquid Densities, ρ, Heats of Vaporization, ΔH_{vap}, and Hydration Free Energies, ΔG_{hyd}, as a Function of the Two Coupling Parameters λ_{PC} and λ_{LJ}[a]

	ρ				
	λ_{PC}				
λ_{LJ}	0.001	0.002	0.01	0.02	0.1
0.000	**0.90**	0.91	0.93	0.93	0.92
0.025	0.89	0.90	0.91	0.91	0.90
0.050	0.87	**0.87**	0.89	0.89	0.89
0.075	0.84	0.86	0.87	0.88	**0.87**
0.100	0.83	0.85	0.86	0.87	0.85
	ΔH_{vap}				
	λ_{PC}				
λ_{LJ}	0.001	0.002	0.01	0.02	0.1
0.000	**13.76**	14.56	16.45	16.56	13.24
0.025	13.51	14.17	15.67	16.04	12.90
0.050	13.28	**13.71**	15.21	15.27	12.85
0.075	12.88	13.49	14.64	14.93	**12.78**
0.100	12.77	13.36	14.34	14.63	12.71
	ΔG_{hyd}				
	λ_{PC}				
λ_{LJ}	0.001	0.002	0.01	0.02	0.1
0.000	**−7.34 ± 0.40**	−7.39 ± 0.63	−8.38 ± 0.25	−8.44 ± 0.03	−6.34 ± 0.18
0.025	−6.65 ± 0.34	−6.75 ± 0.04	−8.00 ± 0.29	−7.92 ± 0.27	−6.05 ± 0.11
0.050	−6.14 ± 0.14	**−6.73 ± 0.14**	−7.10 ± 0.27	−7.27 ± 0.20	−6.03 ± 0.20
0.075	−5.72 ± 0.32	−6.37 ± 0.38	−6.92 ± 0.09	−7.39 ± 0.18	**−5.49 ± 0.13**
0.100	−5.43 ± 0.41	−5.88 ± 0.10	−6.47 ± 0.56	−6.48 ± 0.21	−5.25 ± 0.19

[a]Figures in bold highlight the three MTP models that were retained for further study. All units are in kcal/mol, Å, and g/cm^3. The errors of the mean on the computed densities and heats of vaporization are 0.01 g/cm^3 and 0.05 kcal/mol, respectively, while they are mentioned explicitly for the hydration free energies.

Multiple conformations of NMAH were included in the fit to allow for better parameter transferability.[28,41,42] To ensure consistency between the CGenFF PCs and the fitted MTPs, each monopole was constrained to deviate at most by an amount λ_{PC} from the reference value (i.e., provided by CGenFF). Effectively, larger values of λ_{MP} will provide more flexibility—and thus better fits—at the expense of consistency with the reference PCs.

Any modification of the electrostatics will *de facto* require a reparametrization of the LJ coefficients. As the constraints on MTPs aim at fine-tuning the original force field, a method to adjust the LJ coefficients to balance changes due to the electrostatics is described in the following. To better illustrate the need for LJ reparametrization, Table 2 reports three standard thermodynamic observables used in force-field parametrization—pure-liquid density, ρ, heat of vaporization, ΔH_{vap}, and hydration free energy, ΔG_{hyd}—for different force fields with increasing λ_{PC} while keeping the LJ coefficients intact (i.e., λ_{LJ} = 0.000; the meaning of this parameter will be explained below). While ρ remains virtually identical throughout the range of λ_{PC} studied, ΔH_{vap} and ΔG_{hyd} strongly increase and decrease, respectively—except for the case λ_{PC} = 0.1, where the maximum charge deviation becomes so large that the "corrective" nature of the MTPs breaks down. While no systematic study has so far been reported, a much more pronounced dependence of ΔH_{vap} and ΔG_{hyd} on the LJ radius parameters, $R_{min}/2$, was observed compared to the well depth ε. Compensating for the two clear trends found in ΔH_{vap} and ΔG_{hyd} as a function of λ_{PC} was achieved by *increasing* the $R_{min}/2$ parameters, in agreement with previously reported MTP reparametrizations.[27,43] Ideally, one would proceed by rescaling the LJ radius of each atom type independently. This is neither practical nor desirable, as it would require a high-dimensional parametrization for an underdetermined problem. On the other hand, not all atom types should be rescaled by the same amount λ_{LJ}, given that the fit will typically assign MTPs quite heterogeneously. Here, to each atom type, a relative weight measured by the norm of its dipole, $\mu^{(i)}$, and quadrupole, $\mathbf{Q}^{(i)}$, coefficients is assigned. The strength of atom type i is quantified by measuring its MTP interaction with a charge q placed at a distance R

$$E_i = \frac{1}{4\pi\varepsilon_0}\left(\frac{|\mu^{(i)}|q}{R^2} + \frac{|\mathbf{Q}^{(i)}|q}{R^3}\right) \quad (2)$$

Because the present work focuses on solute−solvent interactions, $R = R_{min}^{(i)}/2 + R_{min}^{wat}/2$ is used, where $R_{min}^{wat}/2$ = 1.8 Å is roughly the LJ radius parameter of TIP3P oxygen. Further, to alleviate artifacts arising from unreasonably small hydrogen radii (e.g., amide hydrogen in CGenFF's NMAH), the atom's radius is set to at least $r_{min}/2$ = 0.8 Å, such that

$$R = \max\left(R_{min}^{(i)}/2, r_{min}/2\right) + R_{min}^{wat}/2$$

As E_i is used as a proxy to weigh the contribution of atom type i, the precise value of q is irrelevant, since it only contributes an overall prefactor. Hence, the weight w_i of atom type i has the form

dx.doi.org/10.1021/jp5011692 | J. Phys. Chem. B 2014, 118, 8135−8147

$$w_i = \frac{1}{R^2}\left(|\mu^{(i)}| + \frac{|\mathbf{Q}^{(i)}|}{R}\right) \tag{3}$$

Overall, the relative weight w_i was computed with the absolute coupling parameter λ_{LJ} to increase the LJ radius parameter of atom type i

$$R^{(i)}_{min}/2 = R^{(i)}_{min}/2\left(1 + \lambda_{LJ}\frac{w_i}{\max_j w_j}\right) \tag{4}$$

Data Analysis. Among the eight response functions $R_1(t_3, t_2, t_1)$ to $R_8(t_3, t_2, t_1)$ that survive the rotating wave approximation, $R_1(t_3, t_2, t_1)$ to $R_6(t_3, t_2, t_1)$ correspond to the 2D IR experiment.[1,44] The response functions can be determined directly from sufficiently long MD simulations. Provided that the underlying frequency distribution $P(\omega(t))$ is Gaussian-shaped and the rotational and vibrational parts which contribute to the spectroscopic signal can be separated, the response functions can be evaluated through a cumulant expansion truncated at second order. In the following, this is assumed to hold, although exceptions including water[1] or cyanide are known to exist.[45,46] The six response functions are

$$\begin{aligned} R_{1,2,3}(t_3, t_2, t_1) &= \sum_{n=1}^{3} R_n(t_3, t_2, t_1) \\ &= \imath\mu_{01}^4\left[e^{-\imath\omega_{01}(t_3-t_1)} - e^{-\imath(\omega_{01}-\Delta)t_3-\omega_{01}t_1}\right] \\ &\quad \times e^{-g(t_1)+g(t_2)-g(t_3)-g(t_1+t_2)-g(t_2+t_3)+g(t_1+t_2+t_3)} \\ R_{4,5,6}(t_3, t_2, t_1) &= \sum_{n=4}^{6} R_n(t_3, t_2, t_1) \\ &= \imath\mu_{01}^4\left[e^{-\imath\omega_{01}(t_3+t_1)} - e^{-\imath(\omega_{01}-\Delta)t_3+\omega_{01}t_1}\right] \\ &\quad \times e^{-g(t_1)-g(t_2)-g(t_3)+g(t_1+t_2)+g(t_2+t_3)-g(t_1+t_2+t_3)} \end{aligned} \tag{5}$$

where t_1, t_2, and t_3 are delay times, Δ is the anharmonic shift between the fundamental and the first vibrationally excited state, i.e., $\Delta = \omega_{01} - \omega_{12} = 12\ cm^{-1}$,[17] and $g(t)$ is the line shape function obtained from the double integration of the FFCF

$$g(t) = \int_0^t \int_0^{\tau'} d\tau' d\tau'' \langle \delta\omega_{01}(\tau'')\delta\omega_{01}(0)\rangle \tag{6}$$

The FFCF, $C(t)$, is determined from the frequency trajectory $\omega(t)$ according to

$$\begin{aligned} C(t) &= \langle \delta\omega(t_0)\delta\omega(t_0 + t)\rangle_{t_0} \\ &= \langle (\omega(t_0) - \bar{\omega})(\omega(t_0 + t) - \bar{\omega})\rangle_{t_0} \end{aligned} \tag{7}$$

If the FFCF is fitted to a suitably parametrized expression, e.g.,

$$C(t) = a_1 \exp(-t/\tau_1) + a_2 \exp(-t/\tau_2) + a_3 \exp(-t/\tau_3) \tag{8}$$

$g(t)$ can be calculated analytically.[1] Alternatively, $g(t)$ can be obtained through numerical integration.[46]

The finite lifetime of the vibrationally excited state T_1 affects the line shape of the 2D IR signal. This is taken into account phenomenologically by multiplication of the response functions R_i by appropriate factors which for R_1, R_2, R_4, and R_5 are

$$\exp\left(-\frac{t_1 + 2t_2 + t_3}{2T_1}\right) \tag{9}$$

and

$$\exp\left(-\frac{t_1 + 2t_2 + 3t_3}{2T_1}\right) \tag{10}$$

for R_3 and R_6. For NMAD in D_2O, the value $T_1 = 0.45$ ps is used.[17] From the response functions $R_{1,\ldots,6}$, the associated 2D IR frequency-domain spectrum is calculated via a double Fourier transform over t_1 and t_3:[1]

$$S(\omega_3, t_2, \omega_1) = \int_0^\infty \int_0^\infty \sum_n R_n(t_3, t_2, t_1) e^{\imath\omega_1 t_1} e^{\imath\omega_3 t_3}\, dt_1\, dt_3 \tag{11}$$

The purely absorptive 2D IR spectra

$$R_{abs}(\omega_1, \omega_3) = \Re(R_r(-\omega_1, \omega_3) + R_{nr}(\omega_1, \omega_3)) \tag{12}$$

is the real part of the sum of the rephasing, R_r, and nonrephasing signal, R_{nr}, where the negative sign in front of ω_1 in R_r is pointed out. Using this method, spectra were obtained for waiting times t_2 ranging from 0 to 10 ps.

To obtain the frequency trajectory $\omega(t)$, NMA is displaced along the corresponding normal mode for each frame along the trajectory. In the procedure employed here, the NMA structure was first optimized in the gas phase. Next, vibrational frequencies are computed. Gaussian 03 provides the L matrix[47] consisting of the normal mode vectors. This matrix needs to be completed by the six elements corresponding to the degrees of freedom of translation and rotation of the whole molecule. During the MD simulations in solution, the NMA structure was fixed at its optimized QM geometry. The effect of a rigid chromophore will be scrutinized further in the Discussion below. As the QM optimized structure is kept frozen during the simulations, the displacement along the normal mode of interest can be performed almost directly:

$$Q = (0, \ldots, 0, \delta q_k, 0, \ldots, 0)^T \tag{13}$$

where δq_k is the normal mode displacement and Q the normal mode vector. The displaced coordinates along the normal mode

$$\tilde{X} = M^{-1/2}LQ + X \tag{14}$$

are determined from X, the optimized Cartesian coordinate matrix of NMA, and M is the mass matrix.

For each configuration of the trajectory, NMA is displaced along the C═O normal mode. The equilibrium C═O separation is at 1.22 Å, and the minimum and maximum separations are 1.11 and 1.38 Å, respectively. This range covers energies of up to 10 000 cm^{-1} above the minimum energy and compares with an expected 2500 cm^{-1} for the one quantum in the C═O normal mode. This procedure yields a one-dimensional potential energy curve which is subsequently fitted and for which the stationary states are determined from solving the 1D Schrödinger equation using the LEVEL program.[14]

RESULTS

First, the performance of the different MTP parametrizations for condensed-phase properties is reported. Then, the 2D IR spectra using the various representations of the intermolecular interactions are discussed and compared with experiment. Finally, the H-bond structuring and dynamics around the solute is investigated. As only small differences between the spectroscopy of NMAH in H_2O and NMAD in D_2O are

dx.doi.org/10.1021/jp5011692 | J. Phys. Chem. B 2014, 118, 8135−8147

expected, both systems are discussed. However, direct comparison is only made for NMAD in D_2O.[17,48]

The MTP Force Field. Table 2 reports the impact of λ_{LJ} on the three thermodynamic parameters ρ, ΔH_{vap}, and ΔG_{hyd}. Increasing the coupling parameter systematically increases ρ and ΔH_{vap}, while it decreases ΔG_{hyd}. Among those, three force-field parameter sets were chosen that reproduced well the results obtained with CGenFF, thereby ensuring a proper correction to the original force field and alleviating any artifact due to systematic errors. Calculations with CGenFF yielded ρ = 0.91 g/cm^3, ΔH_{vap} = 13.90 kcal/mol, and ΔG_{hyd} = −6.70 ± 0.15 kcal/mol. Table 2 displays the selected force fields in bold, where increasing λ_{PC} unsurprisingly required larger λ_{LJ}. Therefore, the three selected MTP models will be referred to in the rest of the article as follows: MTPW (λ_{PC} = 0.001), MTPM (λ_{PC} = 0.002), and MTPS (λ_{PC} = 0.1), where "W", "M", and "S" stand for weak, medium, and strong multipoles, respectively. The parametrizations are provided in the Supporting Information.

2D-IR Spectra from Point Charge Force Fields. In what follows, all spectra are computed as described in the Computational Methods section. Simulations were carried out for NMAH in H_2O and NMAD in D_2O, employing fixed and fluctuating PC models and three different MTP models, respectively. From the equilibrium simulations, the frequency trajectory $\omega(t)$ for the normal mode corresponding to the C═O stretch is determined for 2×10^6 snapshots, separated by 5 fs, and the corresponding FFCF is computed. Figure 4

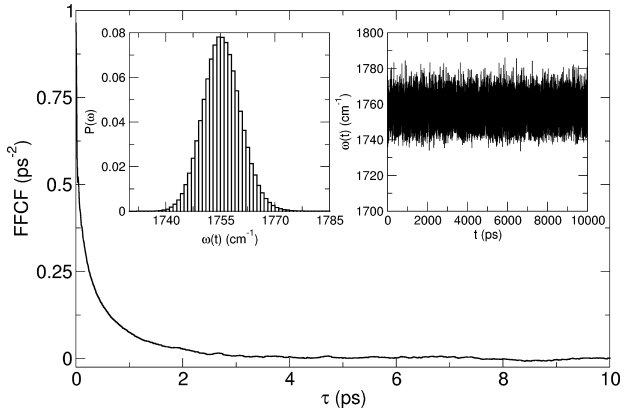

Figure 4. FFCF as a function of lag time for NMAH/FPC in TIP3P water. Insets: frequency of vibration as a function of simulation time and probability distribution of the frequency of vibration for NMAH in TIP3P water.

reports the frequency trajectory from a 10 ns simulation, the distribution $P(\omega)$, and the FFCF for NMAH in H_2O with the FPC model. The frequency distribution is centered around 1755 cm^{-1}, which is red-shifted by −19 cm^{-1} compared to the gas phase frequency at 1774 cm^{-1}. Such a red shift has also been observed experimentally, although the magnitude of the shift is larger (−85 cm^{-1}) than that found from the present simulations.[35] The distribution is close to Gaussian (which could be quantified by a quintile−quintile plot), and the FFCF is found to rapidly decay toward $C(t) = 0$ on a time scale of less than 10 ps.

Corresponding FFCFs for all systems and FF parametrizations investigated are summarized in Figure 5 together with fits to a phenomenological expression. In most cases, the FFCFs

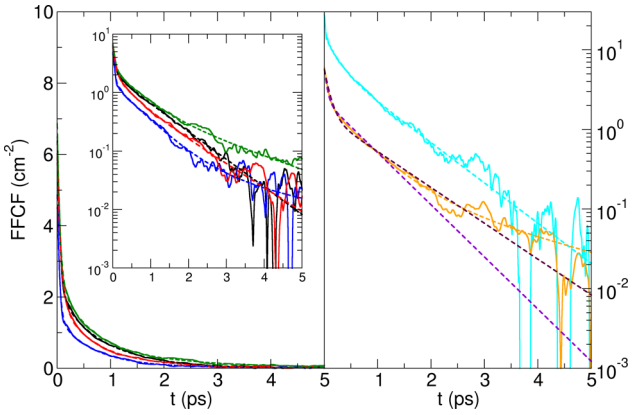

Figure 5. FFCF as a function of lag time (solid line) and the corresponding fit (dashed line) for different models. Left: comparison between the FFCFs for NMAH in H_2O for CGenFF (black) and the multipole models: MTPW (blue), MTPM (green), and MTPS (red). Right: comparison between the FFCFs of FPC (cyan) and MTPS (orange) for NMAD in D_2O.

again decay on the 10 ps time scale with occasional rebounds, specifically when using a fluctuating point charge model for NMAD in D_2O. For the first ∼4 ps, the decay is smooth after which the FFCFs fluctuate. Most of these variations at longer evolution time can be suppressed by extending the simulation time, and it should be emphasized that they are only observable in a semilog representation of the data.

Frequency−frequency correlation functions of other chromophores sometimes exhibit more or less pronounced anticorrelations at short times.[46,49,50] This is not observed in the present simulations. In simulations of CN^- in D_2O,[46] a pronounced anticorrelation at short times ($t \approx 50$ fs) was found. Also, in simulations of HOD in D_2O, such a feature was observed with a corresponding time scale of $t \approx 38$ fs which was attributed to dynamics of the hydrogen-bonded species.[49] Similarly, simulations for azide in D_2O observed such signatures[50] which are absent in any of the FFCFs for the systems considered here. The degree to which such oscillatory features in the FFCF at short times are present has been phenomenologically linked to the strength of the solute−solvent H-bond at the oscillator site probed. As this is expected to decrease in going from CN^-, N_3^-, H_2O to C═O_{NMA}, the observed behavior in the FFCF would be consistent with such an interpretation.

Fitting the FFCF to a sum of decaying exponentials has the advantage that the line shape function can be evaluated in closed form. Such fits including three time scales τ_1−τ_3 are shown in Figure 5 together with the raw data, and the amplitudes and time scales characterizing the FFCF are summarized in Table 3. The behavior up to t = 4 ps is faithfully captured by such an expression, whereas at longer times deviations can occur. However, it should be emphasized that the logarithmic scales overemphasize the deviations of the fit from the data and the quality of the fits is comparable to or even better than in previous studies.[46] For the fluctuating point charge models, three time scales ranging from a few 10 fs to 1 ps are found. This is also the case for the standard CGenFF parametrization. Fitting to only two time scales while keeping the short time scale at 50 fs (as was done in the analysis of the experiments)[48] yields a second decay time of τ_2 = 0.7 ps while assuming a short time scale of 100 fs makes τ_2 slightly larger.

dx.doi.org/10.1021/jp5011692 | J. Phys. Chem. B 2014, 118, 8135−8147

Table 3. Parameters of a Tri-Exponential Fit of the FFCFs[a]

	a_1 (cm^{-2})	t_1 (ps)	a_2 (cm^{-2})	t_2 (ps)	a_3 (cm^{-2})	t_3 (ps)
CGenFF	4.17	0.052	0.31	0.300	1.89	0.920
FPC	12.01	0.017	9.02	0.192	6.12	0.934
FPC(−10%)	12.00	0.017	7.53	0.191	6.15	0.958
FPC(+10%)	12.52	0.012	9.06	0.183	4.10	0.968
FPC(D)	13.02	0.021	7.58	0.217	6.79	0.860
MTPW	3.47	0.043	1.32	0.666	0.06	3.269
MTPM	4.37	0.053	1.80	0.577	0.65	1.918
MTPS	3.89	0.065	1.04	0.417	1.01	1.067
MTPS(D)	3.92	0.065	1.86	0.615	0.23	2.446
sim.[19]		0.06				0.66
exp.[48]		(0.05−0.1)				1.6
exp.[19]		0.01				1.0

[a]The short time scale in ref 48 (50−100 fs) was not explicitly fitted but estimated in the experimental work; a δ-pulse was assumed in the fit. The amplitudes a_i are discussed in the text.[48]

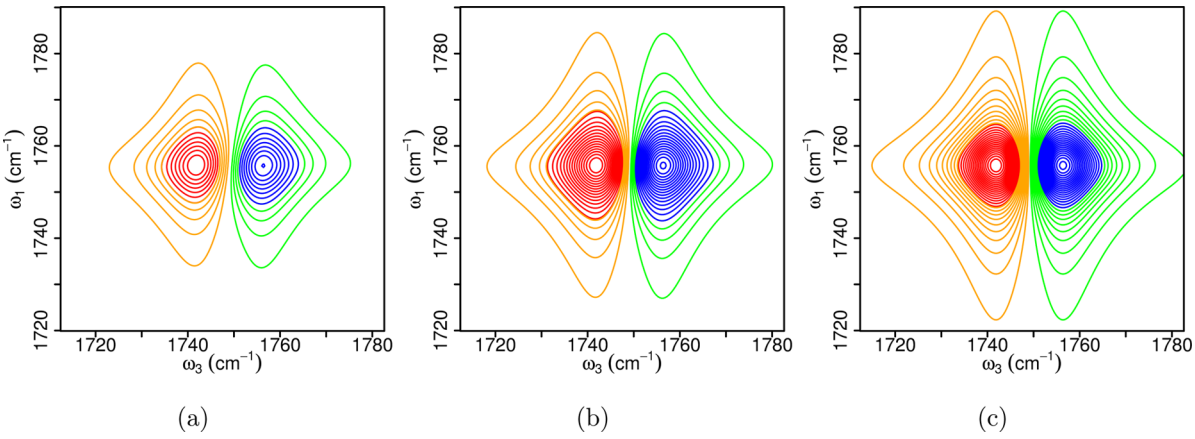

Figure 6. Simulated 2DIR spectrum of the amide I band of NMAH in TIP3P water from the FPC model at different delay times: (a) t_2 = 0.01 ps, (b) t_2 = 0.5 ps, (c) t_2 = 10 ps.

The line shape function $g(t)$ is computed from the FFCFs, which is used to determine the rephasing and nonrephasing response functions R_1, ..., R_6—the basic ingredients of any 2D IR spectrum. 2D IR spectra are reported in Figure 6 for varying delay times t_2 ranging from 0.01 to 10 ps. A sometimes convenient measure for the FFCF is to consider the center line slope which characterizes the time scale on which frequency fluctuations decorrelate (i.e., spectral diffusion time scale).[51] Hence, the CLS reflects the time scale of the solvent's (re)orientational dynamics around the solute. The CLS can be obtained directly from experiment[52] and be compared with simulations.[46] Analysis of the CLS (see Figure 7) in the present case reveals similar decay times as that found for the FFCF. Specifically, the CLS also exhibits one to two relaxation times which reflects the time evolution of the FFCF (Table 4).

2D-IR Spectra from Multipolar and Optimized Force Fields. In order to quantify the influence of more refined representations of the electrostatic interactions, simulations were carried out for different MTP parametrizations of the force fields. They include the MTPW, MTPM, and MTPS models. These additional simulations were also motivated by the recent finding that fixed PC force fields can be unsuitable to correctly capture the solvent dynamics around a chromophore.[46] When multipolar representations for the intermolecular interactions are employed, not only spectroscopic but also thermodynamic and dynamical observables are considerably better described. Hence, simulations and analysis for NMA(H/D) in $(H/D)_2O$ were carried out with different parametrizations of MTP FFs. Three sets of multipoles are used: "weak" (W), "medium" (M), and "strong" (S); see the Computational Methods section and the Supporting Information for parametrizations. The rationale behind such an

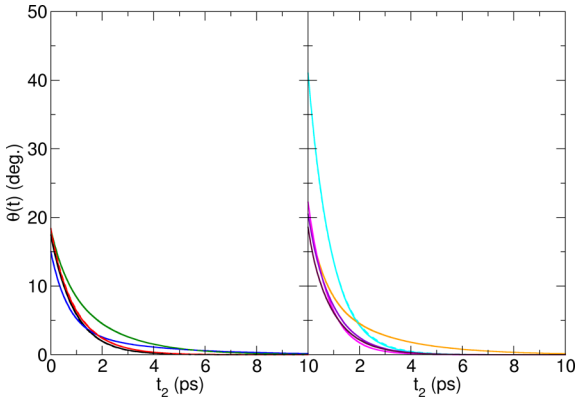

Figure 7. Center line slope (CLS) as a function of the delay time t_2 for NMA in TIP3P water. (left panel) NMAH in H_2O: CGenFF (black), MTPW (blue), MTPM (green), and MTPS (red). (right panel) NMAD in D_2O: FPC (cyan), MTPS(D) (orange), vdW modifications for NMAH in H_2O: FPC(−10%) (violet) and FPC(+10%) (maroon). The solid line corresponds to the data and the dashed lines to the fit which overlap in most cases.

dx.doi.org/10.1021/jp5011692 | J. Phys. Chem. B 2014, 118, 8135−8147

Table 4. Parameters of the Mono- or Bi-Exponential Fit of the CLS Decay

	a_1	t_1 (ps)	a_2	t_2 (ps)
FPC	1.00	0.80		
FPC(D)	1.00	0.90		
CGenFF	1.00	0.91		
MTPW	0.75	0.66	0.25	3.24
MTPM	0.32	0.57	0.68	1.90
MTPS	0.15	0.45	0.85	1.07
MTPS(D)	0.54	0.62	0.46	2.43
exp.[17]	0.80	0.45	0.20	4.0
exp.[48]	1.00	0.90		

approach is the observation that a multipolar representation of a molecular electron density is not unique. Hence, different multipolar FFs are likely to equally well describe the electrostatic potential around a molecule. To each such MTP representation, a separate set of van der Waals parameters needs to be fitted, for example, by comparing with condensed-phase/thermodynamic properties, as was done for the data in Table 2.

For comparing the different multipolar models, simulations of NMAH/D in H_2O and D_2O were at least 10 ns long and the data was stored every 5 fs. Again, NMAH was kept frozen during the simulations and the vibrational frequencies of the C═O normal mode were obtained according to the method described in the previous section.

Figure 5b reports FFCFs for NMAD in D_2O for the fluctuating point charge and the MTPS models together with fits to three- and two-exponential decays. As can be seen for the FFCF for the MTPS model, a three-exponential decay better reproduces the raw data with corresponding time scales of τ_1 = 0.07 ps, τ_2 = 0.62 ps, and τ_3 = 2.45 ps. Assuming two time scales and fixing the short time scale to τ_1 = 0.05 or 0.1 ps yields τ_2 = 0.66 or 0.97 ps, both of which are somewhat shorter than the experimentally determined τ_c = 1.6 ps[48] or agree quite closely with it $\tau_{c,3}$ = 0.98.[19] The amplitudes of the long time components are typically smaller, except for the point charge models, whereas those for the intermediate time scales are somewhat larger; see Table 3. Overall, the amplitudes of the FFCFs are smaller than those observed experimentally, which suggests that the line widths of the 1D spectra are too narrow. Fits of the FFCF to two time scales as done for the experimental data[48] yield amplitudes of the slower component τ_2 between Δ_1 = 1 cm^{-1} and $\Delta_1 \approx$ 3 cm^{-1} for MTP and FPC models, respectively. They compare with Δ_1 = 9 cm^{-1} from experiment.[48] Some of the differences are probably related to the approximation of a rigid NMA(H/D) chromophore. However, it is worthwhile to mention that the computed FFCF for $(Ala)_3$ has a maximum amplitude $C(t = 0)$ = 10 cm^{-2} which yields $\Delta_1 \approx$ 3 cm^{-1} and compares with an experimentally determined value of $\Delta_1 \approx$ 11 cm^{-1}.[48]

The weights of the different components of the FFCFs are 16, 12, and 9 cm^{-1},[48] which compare with the largest amplitudes from the FPC model of 3.6 and 2.6 cm^{-1} for the same decay times. Regardless of the absolute amplitude which is about 4 times smaller than the experimental data, the ratio between the different component is of the same order of magnitude (1.33 experimentally and 1.38 in the present work). These results show first that most of the features extracted from 2D IR spectra can be reproduced adequately by using improved force fields. Specifically, they already provide time scales in good agreement with experimental results.

In previous studies,[39,43,46] a range of experimental observables has been found to be sensitive to the parametrization of the van der Waals terms. In particular, the dependence of the physical observables on van der Waals ranges has been considered. This primarily affected thermodynamic and dynamical quantities, not so for the spectroscopy. Rescaling all van der Waals radii of the chromophore atoms by ±10% and repeating the 10 ns simulations did not lead to pronounced differences in the decay times of the FFCFs.

Solvent Structure around the Chromophore. Atomistic simulations offer the means to investigate a number of properties difficult to obtain from experiment. Quantities of interest include the solvent structure, the topology and dynamics of the H-bonded network, and the energy relaxation pathways. In the following, the trajectories are used to probe the solvent structure around the C═O oscillator and the H-bonded network.

Figure 8 shows the pair-correlation function between the oxygen atom of the carbonyl group of NMA and the O atom of

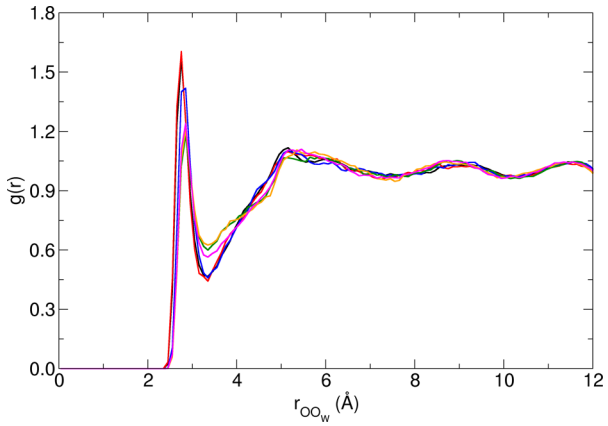

Figure 8. Pair correlation function $g_{OO}(r)$ between the O atom of the C═O group and the O atom (OW) of water for different models: FPC (magenta), MTPW (blue), MTPM (green), MTPS (red), MTPS(D) (orange).

water molecules. For all models, the pair correlation function exhibits a first sharp peak at 2.8 Å, characteristic of a first hydrogen-bonded shell of water. It then exhibits a depletion until the second weak peak at about 5 Å with a minimum at 3.5 Å where the average number of water molecules is 3. The pair correlation function then fluctuates around 1, presenting a correlation, though weak, even until a distance of 12 Å. The first peak and the following depletion zone depend slightly on the model used, specifically their van der Waals parameters. As the MTP models use larger vdW radii (up to 7.5%), the first correlation peak is shifted toward larger distances with a smaller correlation.

Figure 9 shows the isocontour of water density around NMAH for two solute models: CGenFF and MTPS. In both cases, three main regions can be distinguished: (i) a relatively high density region close to the molecule (within the first 3.5 Å) corresponding to the first solvation shell, (ii) a region of moderate density at distances within 5−8 Å corresponding to a second solvation shell, and finally (iii) beyond 8 Å a region of more uniform water distribution corresponding to the recovery of bulk structure. Within the first solvation shell, there are some

dx.doi.org/10.1021/jp5011692 | J. Phys. Chem. B 2014, 118, 8135−8147

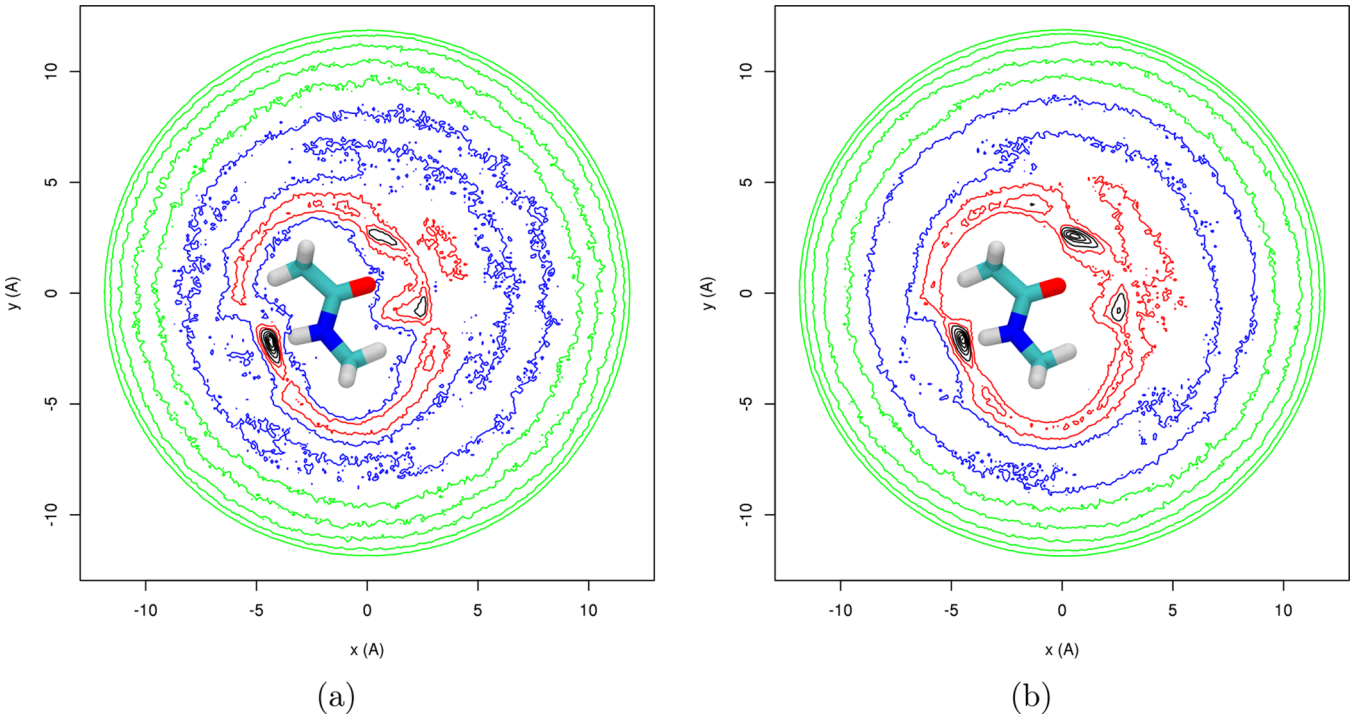

Figure 9. Density plot of water (OW) around the O atom of NMA. NMA is in the (x, y) plane, and the O atom is at the origin. Density is color-coded as follows: green ($\rho \leq 0.25$), blue ($0.30 \leq \rho \leq 0.35$), red ($0.40 \leq \rho \leq 0.45$), and black ($\rho \geq 0.50$). NMA is shown in order to indicate qualitatively the position of the molecule with an arbitrary scale. (a) CGenFF model, (b) MTPS.

specific areas of high density corresponding to H-bonding sites: two around the O atom of NMA and one in front of NMA's NH group. Like the pair-correlation functions, the density exhibits solvation shells at larger distances when an MTP model is used. Multipoles, especially on the carbonyl group, have a strong effect on the nearby water structure, as the high local densities around the O atom are enhanced together with water density beyond them. This is connected to the accurate description of the dipole and quadrupole moments on the C═O group, which account for the lone pairs on the O atom.

Figure 10 shows the density map of the angle between the O atom of $C{=}O_{NMA}$ and the water's H_W and O_W atoms against the distance between O and H_W for the FPC and MTPS models. The density is limited to water molecules for which at least one atom is present within 3.5 Å of NMA's O atom. This distance has been chosen according to the first minimum of the pair-correlation function.

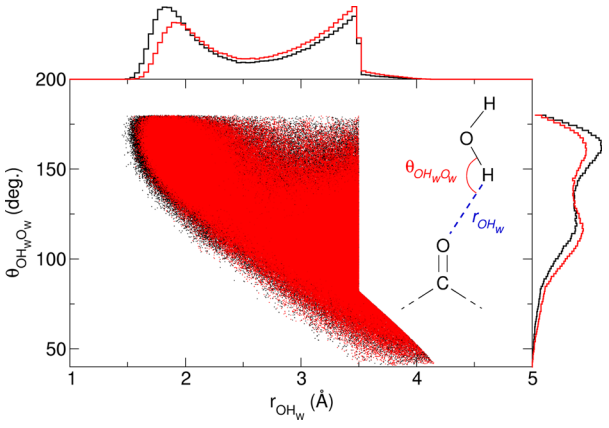

Figure 10. Density map of the $O_{NMA}H_WO_W$ angle against the $O_{NMA}H_W$ distance between the O atom of the C═O group and water molecules within a radius of 3.5 Å around the O for two models: FPC (black) and MTPS (red). On the top and the right side of the figure are shown the projections of the density on the x- and y-axes, respectively.

The two densities—and thus the structure of water—mostly overlap, though a slight shift toward the large $O{-}H_W$ distances is noticeable, due to the increase in van der Waals radii for MTPS. These small features alone cannot explain the important changes in the 2DIR relaxation time between the different electrostatic models.

The relaxation of water around NMA's O atom is characterized as follows: the lifetime, $P(\tau)$, describes the survival time of a water molecule once it enters the first solvation shell (i.e., 3.5 Å) (Figure 11). Further, the residence function describes the probability to find a certain water molecule within the first solvation shell at time $t + \tau$ provided the same molecule was there at time t. This function is obtained from the autocorrelation function (ACF) of

$$H(t) = \begin{cases} 1 & \text{if } r_{OOW} < 3.5 \text{ Å} \\ 0 & \text{otherwise} \end{cases} \quad (15)$$

The H-bond lifetime ($O_{NMA}{-}H_W$) was determined and fitted to a triexponential function. Experimental studies[48] reported a single component, i.e., 2.34 ps, for the H-bond lifetime between water and NMA—the longest time scale observed in our simulations. CGenFF performs satisfactorily with a value of 2.9 ps, and the most accurate results are obtained for FPC(+10%) and MTPS; see Table 5. It is found that these H-bond lifetimes depend strongly on the van der Waals ranges. Also, including MTPs while retaining the CGenFF PCs, without modification of the van der Waals radii (i.e., model MTPW), leads to an increase of the H-bond lifetime by 0.6 ps.

dx.doi.org/10.1021/jp5011692 | J. Phys. Chem. B 2014, 118, 8135−8147

Table 5. Parameters of Tri-Exponential Fit of the Lifetime Functions (O−HW)

	a_1	t_1 (ps)	a_2	t_2 (ps)	a_3	t_3 (ps)
FPC	0.5	0.1	0.2	0.6	0.1	3.3
FPC(D)	0.5	0.1	0.2	0.7	0.1	3.9
FPC(−10)	0.5	0.1	0.2	0.5	0.1	4.6
FPC(+10)	0.5	0.1	0.3	0.4	0.1	2.3
CGenFF	0.5	0.1	0.2	0.5	0.1	2.9
MTPW	0.5	0.1	0.2	0.6	0.1	3.5
MTPM	0.5	0.1	0.2	0.5	0.1	3.4
MTPS	0.5	0.1	0.3	0.5	0.1	2.6
MTPS(D)	0.5	0.1	0.3	0.4	0.1	2.6

However, increase of van der Waals radii compensates this effect of the multipole moments, even for larger ones (MTPS). Similarly, a significant effect of the van der Waals radii is observed for the FPC model, where an increase of 10% of the radii of C═O leads to a lifetime of 2.3 ps while the decrease by 10% leads to a lifetime of 4.6 ps. In other words, the van der Waals radii can tune how much electrostatics affects the interaction strength.

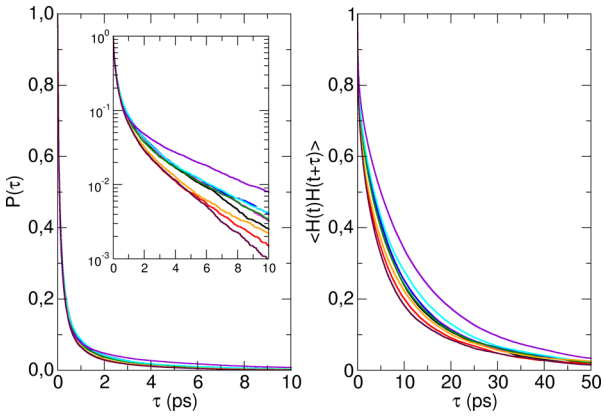

Figure 11. Water lifetimes (HW) around the O atom of NMA: CGenFF (black), FPC (magenta), MTPW (blue), MTPM (green), MTPS (red), FPC(D) (cyan), MTPS(D) (orange), FPC(−10%) (violet), and FPC(+10%) (maroon). (left) Survival time $P(\tau)$ within the first solvation shell (3.5 Å). (right) ACF of $H(t)$ (eq 15) for the first solvation shell (3.5 Å).

DISCUSSION

In this contribution, the possibility to employ validated force fields to understand the 2D IR spectroscopy of solvated *N*-methylacetamide was investigated. Specifically, a unified approach which uses the same computational model for sampling and analyzing the conformational dynamics of the chromophore was adopted. The possibility to realistically determine fundamental data for multidimensional spectroscopies is of particular relevance in the context of larger molecular assemblies, such as peptides and proteins for which generation and analysis of sufficiently long atomistic trajectories becomes an issue. Although frequency maps have paved the way for a meaningful analysis, they have two limitations. First, they need to be gauged for every system, and second, the quality at which they are determined differs from the quality of the computational model employed for sampling the configurations. In other words, a map-based approach has computational and conceptual drawbacks. Typically, one would prefer an approach which treats the energetics, dynamics, and analysis at a unified level. This is what is done for NMA in the present work based on a rigorous MTP force field.

The focus in the present study is on developing and testing a robust and meaningful parametrization of the nonbonded interactions (including PC and MTP electrostatics together with suitable van der Waals parameters) for NMA together with a given water model. As NMA is the fundamental building block of amino acids in the CHARMM force field, the TIP3P water model[25] is the natural choice for the corresponding water model, as this is also the model employed in the parametrization of the CHARMM force field.[34] However, it would also be of interest to test different and potentially more advanced water models[53−60] in a similar fashion. For this, an independent parametrization of NMA will be required so as to best reproduce the condensed-phase properties of NMA together with an alternative water model. Such a study can follow the steps outlined in the present work.

The FFCFs from the present simulations were fitted to two and three time scales as has been done previously.[19,48] The raw data from this study is clearly better represented if three time scales are assumed, which also agrees with previous work on CN^-.[43] However, some caution should be exercised in introducing an increasing number of phenomenological time scales. Nevertheless, the time scales obtained for NMAD in D_2O including a very rapid (50−100 fs) component, and two picosecond components (0.6 and 2.5 ps) can be readily related to the water H-bond dynamics around the chromophore, which provides credibility to the existence of three time scales. Furthermore, the experimentally determined correlation time (τ_c = 1.6 ps) nicely brackets the two computationally determined time scales.

The amplitudes of the FFCFs are generally too small. This suggests that the 1D line widths are too narrow, which is influenced by two factors. First, the chromophore is rigid during the sampling, which, for instance, eliminates the possibility for coupling between the amide-I and amide-II modes—a known phenomenon.[61] Second, the vibrational relaxation time T_1 will affect the line widths as well. Using the $g(t)$ line shape functions from the present simulations within a cumulant approximation gives a 1D line shape, $R_{\text{linear}} \propto |\vec{\mu}_{01}|^2 e^{-i\omega_{01}t} e^{-g(t)}$, where it is assumed that the rotational part can be replaced by a constant—usually set to 1. The full widths at half-maximum (FWHM) for NMAD from such a treatment are 3.0 and 0.7 cm^{-1} for the FPC and MTPS models, respectively. The line widths are underestimated because the $C(0)$ values are too small by approximately an order of magnitude and because the finite lifetime of the v = 1 state was neglected. Accounting for the finite lifetime of T_1 = 0.45 ps increases these FWHMs to 14 and 12 cm^{-1}. This compares with an experimental value of 29 cm^{-1}.[62] As a comparison, a more recent study of the dynamics of NMAD in D_2O based on a parametrized DFT map finds a FWHM of 43 cm^{-1}, which overestimates the experimentally determined value.[63] Conversely, a more elaborate procedure which fits the map to experimental data in different solvents yields a FWHM of 34 cm^{-1}.[64] Evidently, a rigid NMA in the present simulations is too much of a simplification to realistically reproduce the 1D line shape which was appropriately modeled in previous MD simulations.[65] Additional direct comparisons with previous studies of NMAD in D_2O can be made for the pure dephasing time which was determined as 1.12 ps.[17] For MTPS(D), the pure dephasing time ($(\Delta_1^2 * \tau_1)^{-1}$) is ≈1.10 ps if the value of $C(0)$ is scaled by

dx.doi.org/10.1021/jp5011692 | J. Phys. Chem. B 2014, 118, 8135−8147

an order of magnitude (see above) to yield the correct line width. At the more qualitative level, the present simulations correctly capture the elongation of the 2DIR peaks along the diagonal at early evolution times (when the lifetime contribution is excluded in Figure 6) which has also been observed experimentally.[61] This contrasts with a QM/MM study in which this effect was underestimated.[22] The H-bonding lifetimes of D_2O to NMAD are 2.34 ps,[48] which is significantly shorter than that for methanol, for which it was found to be ≈12 ps from simulations and 10−15 ps from experiment.[66] The present simulations find an H-bonding lifetime of 2.6 ps, which is in good agreement with experiment.

The present work establishes that point charge models—static and fluctuating—already provide quite a realistic FFCF, capturing some of the effects observed experimentally. The relaxation times with a PC or FPC model are typically too short compared to experiments irrespective of whether two or three decay times are assumed. Conversely, the various MTP models which are parametrized for solution-phase data perform almost quantitatively compared to experiments with one very rapid relaxation time (50−100 fs) followed by two relaxation times of ∼0.6 ps and ∼2.5 ps. The time scales can be interpreted in terms of H-bonding lifetimes of the water molecules to particular sites around NMA. On the other hand, reliably describing the 1D line shapes is not possible due to the rigid structure of NMA used in the simulations.

It is worthwhile to emphasize that multipolar force fields are not *a priori* expected to provide more insight compared to carefully parametrized PC force fields. The present work highlights this aspect and suggests that, depending on the application, the increased computational effort in simulations with MTP representations is not necessarily justified. On the other hand, comparative studies as the present one are required in order to develop an understanding for the circumstances under which improved force fields are likely to be mandatory.[27,67,68]

If the difficulties to compute meaningful frequency trajectories $\omega(t)$ from simulations with a fully flexible chromophore can be overcome, a number of interesting points can be addressed. Specifically, the coupling between the amide-I and amide-II modes can be included in the analysis. This provides an opportunity to explicitly model the often-missing (or uncontrolled) coupling in standard force fields.[61]

CONCLUSIONS

This work demonstrates that atomistic simulations are suitable to contribute to a detailed understanding of the molecular dynamics of condensed phase systems. For the specific case of NMA in solution, point charge models provide valuable information, although more physically motivated parametrizations including multipoles yield better agreement with experiment, specifically for the time scales (dynamics) involved. It will be of interest to apply such simulations to larger peptides such as $(Ala)_3$, for which corresponding data is available.[48]

ASSOCIATED CONTENT

Supporting Information

Summary of the MTP parametrizations derived from fitting to the condensed phase properties and then used in the simulations with the MTPW, MTPM, and MTPS models. This material is available free of charge via the Internet at http://pubs.acs.org.

AUTHOR INFORMATION

Corresponding Author

*E-mail: m.meuwly@unibas.ch. Phone: +41 (0)61 267 38 21. Fax: +41 (0)61 267 38 55.

Present Address

[§]Max-Planck-Institut für Polymerforschung, Ackermannweg 10, 55128 Mainz, Germany.

Notes

The authors declare no competing financial interest.

ACKNOWLEDGMENTS

The authors gratefully acknowledge financial support from the Swiss National Science Foundation through grant 200021-117810 and the NCCR-MUST. The authors thank Prof. Peter Hamm for fruitful discussions and comments on the manuscript. One of the authors (M.M.) is particularly grateful to Prof. Jim Skinner for introducing him to the field of computational multidimensional spectroscopy.

REFERENCES

(1) Hamm, P.; Zanni, M. *Concepts and Methods of 2D Infrared Spectroscopy*; Cambridge University Press: Cambridge, UK, 2011.

(2) Li, S.; Schmidt, J.; Corcelli, S.; Lawrence, C.; Skinner, J. Approaches for the Calculation of Vibrational Frequencies in Liquids: Comparison to Benchmarks for Azide/Water Clusters. *J. Chem. Phys.* **2006**, *124*, 204110.

(3) Oxtoby, D. W.; Levesque, D.; Weis, J.-J. A Molecular Dynamics Simulation of Dephasing in Liquid Nitrogen. *J. Chem. Phys.* **1978**, *68*, 5528−5533.

(4) Hayashi, T.; Hamaguchi, H. Solvent Induced Dynamic Polarization, Vibrational Dephasing, and Infrared Band Shape of the C═O Stretch Mode of Acetone in Acetonitrile: A New Theoretical Approach. *Chem. Phys. Lett.* **2000**, *326*, 115−122.

(5) Hayashi, T.; Zhuang, W.; Mukamel, S. Electrostatic DFT Map for the Complete Vibrational Amide Band of NMA. *J. Phys. Chem. A* **2005**, *109*, 9747−9759.

(6) Hayashi, T.; La Cour Jansen, T.; Zhuang, W.; Mukamel, S. Collective Solvent Coordinates for the Infrared Spectrum of HOD in D_2O Based on an Ab Initio Electrostatic Map. *J. Phys. Chem. A* **2005**, *109*, 64−82.

(7) Jansen, T. L. C.; Hayashi, T.; Zhuang, W.; Mukamel, S. Stochastic Liouville Equations for Hydrogen-Bonding Fluctuations and their Signatures in Two-Dimensional Vibrational Spectroscopy of Water. *J. Chem. Phys.* **2005**, *123*, 114504.

(8) Corcelli, S. A.; Lawrence, C. P.; Skinner, J. L. Combined Electronic Structure/Molecular Dynamics Approach for Ultrafast Infrared Spectroscopy of Dilute HOD in Liquid H_2O and D_2O. *J. Chem. Phys.* **2004**, *120*, 8107−8117.

(9) Field, M. J.; Bash, P. A.; Karplus, M. A Combined Quantum Mechanical and Molecular Mechanical Potential for Molecular Dynamics Simulations. *J. Comput. Chem.* **1990**, *11*, 700−733.

(10) Gao, J. Hybrid Quantum and Molecular Mechanical Simulations: an Alternative Avenue to Solvent Effects in Organic Chemistry. *Acc. Chem. Res.* **1996**, *29*, 298−305.

(11) Cui, Q.; Karplus, M. Quantum Mechanical/Molecular Mechanical Studies of the Triosephosphate Isomerase-Catalyzed Reaction: Verification of Methodology and Analysis of Reaction Mechanisms. *J. Phys. Chem. B* **2002**, *106*, 1768−1798.

(12) Garcia-Viloca, M.; Nam, K.; Alhambra, C.; Gao, J. Solvent and Protein Effects on the Vibrational Frequency Shift and Energy Relaxation of the Azide Ligand in Carbonic Anhydrase. *J. Phys. Chem. B* **2004**, *108*, 13501−13512.

(13) Hermansson, K.; Knuts, S.; Lindgren, J. The OH Vibrational Spectrum of Liquid Water from Combined Abinitio and Monte Carlo Calculations. *J. Chem. Phys.* **1991**, *95*, 7486−7496.

(14) Roy, R. L. *LEVEL 7.5: a Computer Program to Solve the Radial Schrödinger Equation for Bound and Quasibound Levels*; Waterloo, Ontario, Canada, 2002.
(15) Hamm, P.; Lim, M.; Hochstrasser, R. M. Structure of the Amide I Band of Peptides Measured by Femtosecond Nonlinear-Infrared Spectroscopy. *J. Phys. Chem. B* **1998**, *5647*, 6123−6138.
(16) Rey, R.; Hynes, J. T. Vibrational Phase and Energy Relaxation of CN^- in Water. *J. Chem. Phys.* **1998**, 142−153.
(17) Zanni, M. T.; Asplund, M. C.; Hochstrasser, R. Two-Dimensional Heterodyned and Stimulated Infrared Photon Echoes of N-Methylacetamide-D. *J. Chem. Phys.* **2001**, *114*, 4579−4590.
(18) Hamm, P.; Hochstrasser, R. M. In *Ultrafast Infrared and Raman Spectroscopy*; Fayer, M., Ed.; Marcel Dekker: New York, 2001; pp 273−347.
(19) Decamp, M. F.; Deflores, L.; Mccracken, J. M.; Tokmakoff, A.; Kwac, K.; Cho, M. Amide I Vibrational Dynamics of N-Methylacetamide in Polar Solvents: The Role of Electrostatic Interactions. *J. Phys. Chem. B* **2005**, *109*, 11016−11026.
(20) Bastida, A.; Soler, M. A.; Zuniga, J.; Requena, A.; Kalstein, A.; Fernandez-Alberti, S. Instantaneous Normal Modes, Resonances, and Decay Channels in the Vibrational Relaxation of the Amide I Mode of N-Methylacetamide-D in Liquid Deuterated Water. *J. Chem. Phys.* **2010**, *132*, 224501.
(21) Bastida, A.; Soler, M. A.; Zuniga, J.; Requena, A.; Kalstein, A.; Fernandez-Alberti, S. Hybrid Quantum/Classical Simulations of the Vibrational Relaxation of the Amide I Mode of N-Methylacetamide in D_2O Solution. *J. Phys. Chem. B* **2012**, *116*, 2969−2980.
(22) Jeon, J.; Cho, M. Direct Quantum Mechanical/Molecular Mechanical Simulations of Two-Dimensional Vibrational Responses: N-Methylacetamide in Water. *New J. Phys.* **2010**, *12*, 065001.
(23) Brooks, B. R.; et al. CHARMM: The Biomolecular Simulation Program. *J. Comput. Chem.* **2009**, *30*, 1545−1614.
(24) Vanommeslaeghe, K.; Hatcher, E.; Acharya, C.; Kundu, S.; Zhong, S.; Shim, J.; Darian, E.; Guvench, O.; Lopes, P.; Vorobyov, I.; Mackerell, A. D., Jr. CHARMM General Force Field: A Force Field for Drug-Like Molecules Compatible with the CHARMM All-Atom Additive Biological Force Fields. *J. Comput. Chem.* **2010**, *31*, 671−690.
(25) Jorgensen, W. L.; Chandrasekhar, J.; Madura, J. D.; Impey, R. W.; Klein, M. L. Comparison of Simple Potential Functions for Simulating Liquid Water. *J. Chem. Phys.* **1983**, *79*, 926−935.
(26) van Gunsteren, W.; Berendsen, H. Algorithms for Macromolecular Dynamics and Constraint Dynamics. *Mol. Phys.* **1977**, *34*, 1311−1327.
(27) Bereau, T.; Kramer, C.; Meuwly, M. Leveraging Symmetries of Static Atomic Multipole Electrostatics In Molecular Dynamics Simulations. *J. Chem. Theory Comput.* **2013**, *9*, 5450−5459.
(28) Kramer, C.; Gedeck, P.; Meuwly, M. Atomic Multipoles: Electrostatic Potential Fit, Local Reference Axis Systems and Conformational Dependence. *J. Comput. Chem.* **2012**, *33*, 1673−1688.
(29) Feller, S. E.; Zhang, Y.; Pastor, R. W.; Brooks, B. R. Constant Pressure Molecular Dynamics Simulation: The Langevin Piston Method. *J. Chem. Phys.* **1995**, *103*, 4613−4621.
(30) Allen, M. P.; Tildesley, D. J. *Computer Simulation of Liquids*; Oxford University Press: New York, 1987.
(31) Frisch, M. J.; Trucks, G. W.; Schlegel, H. B.; et al. *Gaussian 03*, revision B.01; Gaussian, Inc.: Wallingford, Connecticut, USA, 2003.
(32) Singh, U. C.; Kollman, P. A. An Approach to Computing Electrostatic Charges for Molecules. *J. Comput. Chem.* **1984**, *5*, 129−145.
(33) Besler, B. H.; Merz, K. M.; Kollman, P. A. Atomic Charges Derived from Semiempirical Methods. *J. Comput. Chem.* **1990**, *11*, 431−439.
(34) MacKerell, A. D., Jr.; et al. All Atom Empirical Potential for Molecular Modeling and Dynamics Studies of Proteins. *J. Phys. Chem. B* **1998**, *102*, 3586−3616.
(35) Kubelka, J.; Keiderling, T. Ab Initio Calculation of Amide Carbonyl Stretch Vibrational Frequencies in Solution with Modified Basis Sets. 1. N-Methyl Acetamide. *J. Phys. Chem. A* **2001**, *105*, 10922−10928.
(36) Nutt, D. R.; Karplus, M.; Meuwly, M. Potential Energy Surface and Molecular Dynamics of MbNO: Existence of an Unsuspected FeON Minimum. *J. Phys. Chem. B* **2005**, *109*, 21118−21125.
(37) Nutt, D. R.; Meuwly, M. Ferric and Ferrous Iron in Nitroso-Myoglobin: Computer Simulations of Stable and Metastable States and their Infrared Spectra. *ChemPhysChem* **2007**, *8*, 527−536.
(38) Mishra, S.; Meuwly, M. Atomistic Simulation of NO Dioxygenation in Group I Truncated Hemoglobin. *J. Am. Chem. Soc.* **2010**, *132*, 2968−2982.
(39) Lee, M. W.; Meuwly, M. On the Role of Nonbonded Interactions in Vibrational Energy Relaxation of Cyanide in Water. *J. Phys. Chem. A* **2011**, *115*, 5053−5061.
(40) Cazade, P.-A.; Meuwly, M. Oxygen Migration Pathways in NO-bound Truncated Hemoglobin. *ChemPhysChem* **2012**, 4276−4286.
(41) Koch, U.; Popelier, P. L. A.; Stone, A. J. Conformational Dependence of Atomic Multipole Moments. *Chem. Phys. Lett.* **1995**, *238*, 253−260.
(42) Kramer, C.; Bereau, T.; Spinn, A.; Liedl, K. R.; Gedeck, P.; Meuwly, M. Deriving Static Atomic Multipoles from the Electrostatic Potential. *J. Chem. Inf. Model.* **2013**, *53*, 3410−3417.
(43) Lee, M. W.; Meuwly, M. Hydration Free Energies of Cyanide and Hydroxide Ions from Molecular Dynamics Simulations with Accurate Force Fields. *Phys. Chem. Chem. Phys.* **2013**, *15*, 20303−20312.
(44) Schmidt, J.; Roberts, S.; Loparo, J.; Tokmakoff, A.; Fayer, M.; Skinner, J. Are Water Simulation Models Consistent with Steady-State and Ultrafast Vibrational Spectroscopy Experiments? *Chem. Phys.* **2007**, *341*, 143−157.
(45) Lascombe, J.; Perrot, M. Structure and Motion in Water - Analysis of Vibrational and Rotational Dynamics of Cyanide Ion in Aqueous-Solution from Infrared and Raman Band Shapes. *Faraday Discuss.* **1978**, *66*, 216−230.
(46) Lee, M. W.; Carr, J. K.; Göllner, M.; Hamm, P.; Meuwly, M. 2D IR Spectra of Cyanide in Water Investigated by Molecular Dynamics Simulations. *J. Chem. Phys.* **2013**, *139*, 054506.
(47) Wilson, E. B., Jr.; Decius, J. C.; Cross, P. C. *Molecular Vibrations - The Theory of Infrared and Raman Vibrational Spectra*; Mcgraw-Hill: New York, 1955.
(48) Woutersen, S.; Pfister, R.; Hamm, P.; Mu, Y.; Kosov, D.; Stock, G. Peptide Conformational Heterogeneity Revealed from Nonlinear Vibrational Spectroscopy and Molecular-Dynamics Simulations. *J. Chem. Phys.* **2002**, *117*, 6833−6840.
(49) Møller, K. B.; Rey, R.; Hynes, J. T. Hydrogen Bond Dynamics in Water and Ultrafast Infrared Spectroscopy: A Theoretical Study. *J. Phys. Chem. A* **2004**, *108*, 1275−1289.
(50) Li, S.; Schmidt, J. R.; Piryatinski, A.; Lawrence, C. P.; Skinner, J. L. Vibrational Spectral Diffusion of Azide in Water. *J. Phys. Chem. B* **2006**, *110*, 18933−18938.
(51) Kwak, K.; Park, S.; Finkelstein, I. J.; Fayer, M. D. Frequency-Frequency Correlation Functions and Apodization in Two-Dimensional Infrared Vibrational Echo Spectroscopy: A New Approach. *J. Chem. Phys.* **2007**, *127*, 124503.
(52) Koziński, M.; Garrett-Roe, S.; Hamm, P. Vibrational Spectral Diffusion of CN^- in Water. *Chem. Phys.* **2007**, *341*, 5−10.
(53) Kumagai, N.; Kawamura, K.; Yokokawa, T. An Interatomic Potential Model for H_2O - Applications to Water and Ice Polymorphs. *Mol. Simul.* **1994**, *12*, 177−186.
(54) Guillot, B. A Reappraisal of What We Have Learnt during Three Decades of Computer Simulations on Water. *J. Mol. Liq.* **2002**, *101*, 219−260.
(55) Jorgensen, W. L.; Tirado-Rives, J. Potential Energy Functions for Atomic-Level Simulations of Water and Organic and Biomolecular Systems. *Proc. Natl. Acad. Sci. U.S.A.* **2005**, *102*, 6665−6670.
(56) Wu, Y.; Tepper, H. L.; Voth, G. A. Flexible Simple Point-Charge Water Model with Improved Liquid-State Properties. *J. Chem. Phys.* **2006**, *124*, 024503.
(57) Kumar, R.; Skinner, J. L. Water Simulation Model with Explicit Three-Molecule Interactions. *J. Phys. Chem. B* **2008**, *112*, 8311−8318.

(58) Vega, C.; Abascal, J. L. F.; Conde, M. M.; Aragones, J. L. What Ice Can Teach Us aboutWater Interactions: A Critical Comparison of the Performance of Different Water Models. *Faraday Discuss.* **2009**, *141*, 251−276.
(59) Szalewicz, K.; Leforestier, C.; van der Avoird, A. Towards the Complete Understanding of Water by a First-Principles Computational Approach. *Chem. Phys. Lett.* **2009**, *482*, 1−14.
(60) Tainter, C. J.; Pieniazek, P. A.; Lin, Y.-S.; Skinner, J. L. Robust Three-Body Water Simulation Model. *J. Chem. Phys.* **2011**, *134*, 184501.
(61) Deflores, L. P.; Ganim, Z.; Ackley, S. F.; Chung, H. S.; Tokmakoff, A. The Anharmonic Vibrational Potential and Relaxation Pathways of The Amide I and II Modes of NMethylacetamide. *J. Phys. Chem. B* **2006**, *110*, 18973−18980.
(62) Eaton, G.; Symons, M. C. R.; Rastogi, P. P. Spectroscopic Studies of the Solvation of Amides with N-H Groups 0.1. The Carbonyl Group. *J. Chem. Soc., Faraday Trans. 1* **1989**, *85*, 3257−3271.
(63) Bloem, R.; Dijkstra, A. G.; Jansen, T. l. C.; Knoester, J. Simulation of Vibrational Energy Transfer in Two-Dimensional Infrared Spectroscopy of Amide I and Amide II Modes in Solution. *J. Chem. Phys.* **2008**, *129*, 055101.
(64) Wang, L.; Middleton, C. T.; Zanni, M. T.; Skinner, J. L. Development and Validation of Transferable Amide I Vibrational Frequency Maps for Peptides. *J. Phys. Chem. B* **2011**, *115*, 3713−3724.
(65) Yang, S.; Cho, M. IR Spectra of N-Methylacetamide in Water Predicted by Combined Quantum Mechanical/Molecular Mechanical Molecular Dynamics Simulations. *J. Chem. Phys.* **2005**, *123*, 134503.
(66) Woutersen, S.; Mu, Y.; Stock, G.; Hamm, P. Hydrogen-Bond Lifetime Measured by Time-Resolved 2D-IR Spectroscopy: N-Methylacetamide in Methanol. *Chem. Phys.* **2001**, *266*, 137−147.
(67) Kramer, C.; Gedeck, P.; Meuwly, M. Multipole-Based Force Fields from Ab Initio Interaction Energies and the Need for Jointly Refitting All Intermolecular Parameters. *J. Chem. Theory Comput.* **2013**, *9*, 1499−1511.
(68) Plattner, N.; Meuwly, M. The Role of Higher CO-Multipole Moments in Understanding the Dynamics of Photodissociated Carbonmonoxide in Myoglobin. *Biophys. J.* **2008**, *94*, 2505−2515.